*Applied Research*

Applied Research

RESEARCH ARTICLE

# Spectroscopic Ellipsometric Investigations on Organic/Inorganic Liquid Surfaces in Mid-IR Range

László Makai[1] | Bálint Fodor[1] | Péter Rutka[1] | Péter Basa[1] | Benjámin Kalas[1] | Alekszej Romanenko[2] | Péter Petrik[2,3]

[1]Semilab Semiconductor Physics Laboratory Co. Ltd., Budapest, Hungary | [2]Institute for Technical Physics and Materials Science, Centre for Energy Research, Budapest, Hungary | [3]Department of Electrical Engineering, Debrecen University, Debrecen, Hungary

**Correspondence:** László Makai (laszlo.makai@semilab.hu)

**Received:** 7 August 2025 | **Revised:** 18 May 2026 | **Accepted:** 31 May 2026

## ABSTRACT

Structural and optical properties of various liquid samples are of particular importance for both chemical and biological applications. These characteristics can be readily obtained from highly accurate, non-destructive ellipsometric measurements in a wide wavelength range. However, for a reliable result, certain technical obstacles must be eliminated for this type of measurement, e.g., excluding the environmental vibrations and providing an aligned liquid surface are both essential. Previously, it was shown that by using an ellipsometric configuration with active pneumatic isolators, it is possible to obtain vital structural information from both liquid-air and liquid-liquid interfaces, revealing nanoscale surface structures. In this work, the method is further extended by incorporating infrared ellipsometry, expanding the accessible spectral range into the mid-infrared region for enhanced surface and compositional analysis.

## 1 | Introduction

Optical properties of various organic/inorganic liquid samples are of particular importance for both chemical and biological applications. These characteristics can be readily obtained from contactless, non-destructive spectroscopic ellipsometry (SE) measurements in a wide wavelength range.

For reliable results, however, technical obstacles must be eliminated, e.g., eliminating environmental vibrations and providing an aligned liquid surface are both necessary. It was shown previously that by using a SE configuration with active pneumatic isolators, it is achievable to obtain vital structural information from both liquid-air and liquid-liquid interfaces, revealing nanoscale surface structures [1].

In this study, the extended capability of the above SE configuration is presented, for which the available wavelength range is extended towards the mid-infrared region down to 600 $cm^{-1}$ wavenumber (up to 16.66 μm). This wavelength domain is of great significance for revealing the chemical composition of the investigated organic/inorganic liquid sample in a label‾free manner with high sensitivity [2]; thus, besides the structural properties and complex refractive index information, additional knowledge regarding the composition can also be obtained. The performance of the proposed ellipsometric configuration is demonstrated with real measurements on bulk liquid samples, e.g., high-purity water, various organic mixtures, and inorganic solutions with several different %ws.

One of the key applications of mid-infrared ellipsometry in liquid measurement could be in the field of biochemistry [3]. For instance, it can be used to measure the concentration of proteins in a solution, or to monitor the binding of molecules to a protein. This can be crucial in drug discovery and development processes.

Moreover, mid-infrared ellipsometry could also be used in the field of petrochemicals to measure the composition of oil mixtures. This can help in optimizing the extraction and refining processes.

Infrared spectroscopic ellipsometry is a reflection-based technique and is therefore inherently sensitive to the air–liquid

boundary from which the reflected beam originates. In this work, the term "surface" refers to the optical modeling of this interface required for accurate fitting of the ellipsometric spectra (including an effective interfacial EMA layer). The study does not aim to independently determine chemically distinct surface-phase optical constants beyond this effective interfacial description.

## 2 | Methods and Materials

Fourier Transform Infrared Ellipsometry (FTIR-SE) [4], which operates in the mid-infrared spectrum, offers several advantages over traditional visible light ellipsometry (Vis SE). The mid-infrared spectrum is sensitive to vibrational and rotational modes of molecules, making FTIR-SE particularly useful for the study of molecular interactions in liquids.

The same set of technical problems must be solved for mid-infrared ellipsometry as for the visible ellipsometry on liquids: eliminating the environmental vibration and aligning the incident plane according to the plane of the liquid surface. In case of the infrared ellipsometry, the challenge is that the stability must be maintained longer as the measurement time is longer than for visible ellipsometry. To address this challenge, pneumatic isolators were utilized to make use of the actuators' set-screws height to tilt the ellipsometer assembly according to the liquid surface Figure 1a. Using this method, the plane defined by the ellipsometer's illumination and detection arms can be aligned with the incidence plane that is perpendicular to the specimen surface, ensuring that the incident beam at angle $\Theta_i$ is equal to the reflected beam $\Theta_r$ reaching the detection arm. During tilt alignment, the sample stage and the Petri dish moved together with the instrument; the liquid surface remained horizontal.

In this study, an advanced version of a SE-2000 spectroscopic ellipsometer was used, provided by Semilab as depicted in Figure 1b. The state-of-the-art SE-2000 system with mid-infrared ellipsometry extension is capable of high-accuracy ellipsometric measurements in the wavelength range of 1.43−16.66 um (600–7000 $cm^{-1}$) [5]. The incidence angle of the probing light can be automatically set in the range of 30° to 90° [5].

The most valuable information that can be obtained from liquid species in the mid-infrared range is not layer thickness but the molecular constitution of the material and its alteration by mixing it with other liquid or solid materials.

Two experimental material systems were selected to investigate the feasibility of mid-infrared ellipsometry measurement on liquid surfaces. First, an ethanol-water system in various concentration mixes, produced from water (purified by Reverse Osmosis with resulting resistivity of 18MOhmcm) to absolute alcohol (purity > 99.8%, analytical grade) in 10w% steps with 0.3w% accuracy.

The second investigated system is the solution of NaCl in water. This system was selected to demonstrate the capabilities of the mid-IR SE configuration, since according to previous results [6], the additional NaCl ions not only perturb the complex refractive index (defined as N = n -ik) of the water, but an additional effect is that the dissolved ions of the NaCl locally distort the random orientation of water molecules and arranges them around the Na+ and Cl- ions [7]. At room temperature, it is known [8] that the solubility of NaCl in water at 25°C is 36.0 g/100 g, so the saturation concentration of this system is 26.47w%. Therefore, a saturated solution could be used as a verification material. The concentration ladder for the NaCl solutions was created with the (0w%=water); 0.5w%; 1w%; 5w%; 10w%, 20w%; and a saturated solution with 26.47w%.

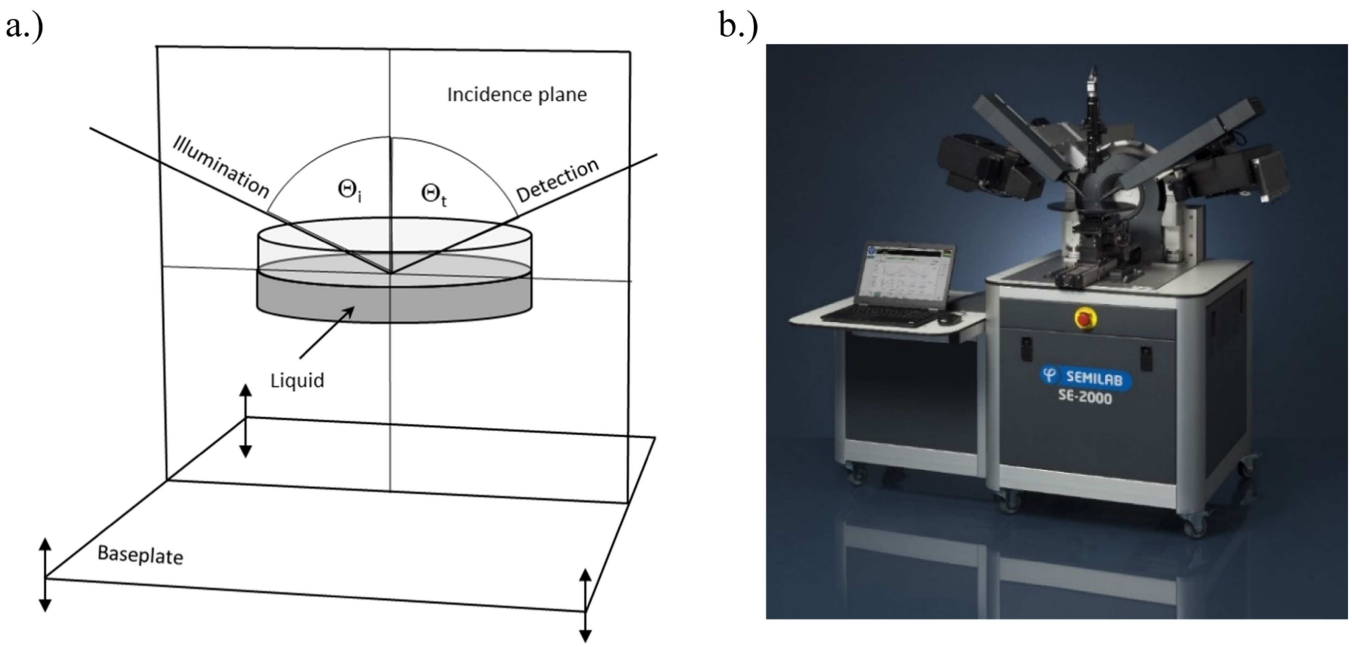


**FIGURE 1** | Schematic view of the measurement setup (a), on the SE-2000 Spectroscopic Ellipsometer (b) from Semilab.

The measurement incidence angle was chosen as 60° because this Angle of Incidence (AOI) is slightly above the Brewster angles of water and ethanol, which maximizes ellipsometric sensitivity while keeping good signal-to-noise, and it remains robust across the mid-IR, where both liquids are weakly to strongly absorbing and their refractive indices are dispersive.

Choosing the AOI 60°, a few degrees above Brewster angle for both liquids, strikes a balance: strong sensitivity, adequate reflected p-intensity for good signal to noise ratio (SNR) and reduces sensitivity to small angle jitters and surface ripples on liquids.

The angle of incidence (AOI) was set using the instrument's alignment system and remained fixed during acquisition; no active feedback control was applied.

The FTIR acquisitions were performed with 32 scans, and 16 $cm^{-1}$ spectral resolution with a liquid nitrogen cooled MCT-A detector. The ellipsometric spectra were acquired over a broad mid-IR range and evaluated by fitting a parametric dispersion model to the full spectral response. Therefore, the selected resolution of 16 $cm^{-1}$ was chosen as a practical compromise, as the analysis is based on broadband model fitting rather than on resolving or assigning individual narrow vibrational lines. Under these conditions, a measurement time of about 4 min offers a practical compromise between maintaining adequate SNR and limiting sample alterations due to evaporation. The specimens were situated in high-purity polystyrene Petri dishes on the ellipsometer stage, exposed to ambient air. Therefore, slight composition changes during acquisition cannot be fully excluded due to evaporation and (for ethanol) water vapor uptake from air. These effects can be most noticeable in the stretching region (around 3000 $cm^{-1}$) and may contribute to small differences compared to literature optical constants obtained under different sample-handling conditions. The ellipsometer was isolated from environmental vibrations using pneumatic isolators. The overall system tilt was aligned with respect to the liquid surface as described above and in [1].

The extracted optical constants obtained from infrared spectroscopic ellipsometry are subject to several sources of uncertainty. Instrumental contributions include measurement repeatability, signal-to-noise limitations, and potential calibration/alignment imperfections. Geometrical factors include incidence-angle setting and the finite opening angle of the probing beam, which introduce angular averaging and can slightly modify the effective ellipsometric response. Modeling-related uncertainties arise from parameter correlations and non-uniqueness in multi-parameter dispersion models (e.g., multi-oscillator representations), especially if model complexity is increased.

To ensure robustness, general robustness checks were performed (see detailed fitting strategy in Results section).

The reported conclusions are based primarily on relative trends in n and k under controlled composition variation, which remain stable within the estimated uncertainty.

### 2.1 | Liquid-Surface Stability and Role of Pneumatic Isolation

Reliable ellipsometric measurements on free liquid surfaces require effective suppression of surface motion. In the present setup, liquid-surface stability was achieved primarily through mechanical isolation of the entire instrument rather than by directly modifying or damping the liquid itself. The ellipsometer, sample stage, and Petri dish were mounted on active pneumatic isolators, which significantly reduce the transmission of environmental vibrations to the liquid. Although the isolation system does not actively control the fluid surface, it effectively suppresses vibration-induced excitations that would otherwise generate or sustain surface ripples during the relatively long acquisition times required for FTIR-based ellipsometry.

No surfactants or surface-active agents were applied, as these would alter the chemical and optical properties of the investigated liquids. After sample placement and instrument tilt alignment, measurements were initiated only after visible transient surface disturbances had decayed. Surface stability was not monitored by a dedicated sensor; instead, it was assessed indirectly through the repeatability and quality of the ellipsometric spectra. Excessive surface motion would manifest as increased noise, depolarization, or systematic deviations between measured and modeled data, none of which were observed beyond the intrinsic noise level of mid-IR liquid ellipsometry.

The probing beam is quasi-collimated with a spot size on the centimeter scale, such that residual small-amplitude surface height fluctuations are laterally averaged over the illuminated area. Furthermore, measurements were performed at an angle of incidence slightly above the Brewster angle, which provides high sensitivity to optical constants while remaining comparatively robust against small angular perturbations caused by surface undulations. Taken together, these considerations indicate that residual surface ripples do not introduce significant scattering or depolarization artifacts and do not affect the extracted optical constants within the experimental uncertainty.

All measurements were performed under ambient laboratory conditions at room temperature (approximately 22°C–25°C). The relative humidity was not actively controlled but is estimated to have been in the range of 40–60%. No dedicated environmental control or systematic variation of temperature and humidity was implemented. The reported results are therefore based on measurements performed under consistent laboratory conditions, and conclusions rely primarily on relative trends, which remain robust against minor ambient variations.

## 3 | Results and Discussion

The measured and calculated ellipsometry spectra for the two unmixed liquid species are shown in Figure 2. Where α and β denote the Fourier coefficients of the intensity signal obtained during rotation of the analyzer in a rotating analyzer ellipsometry (RAE) system. In the applied system, the stop-analyzer method is used, where spectra are collected at discrete

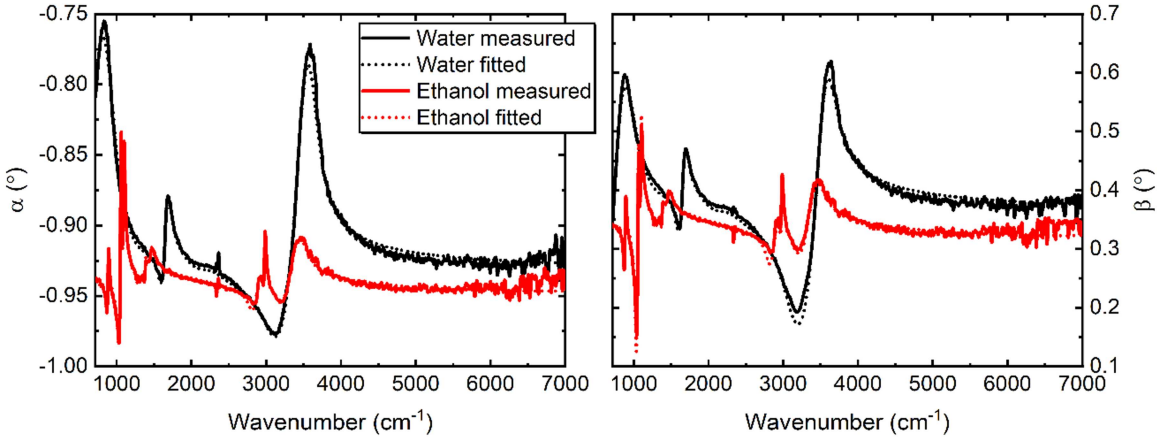


**FIGURE 2** | Measured and fitted ellipsometry spectra of the water and Ethanol.

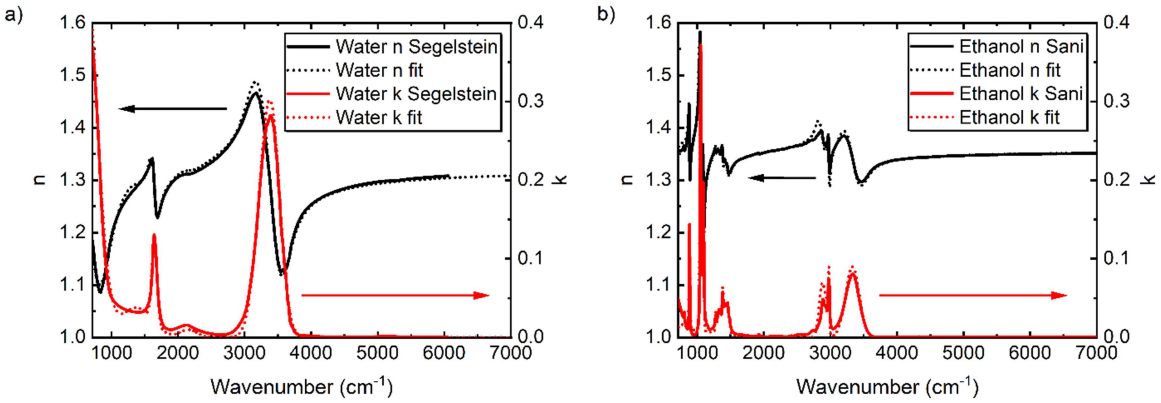


**FIGURE 3** | Comparison of the obtained refractive indices (n) and extinction coefficients (k) extracted from ellipsometric fitting, compared with the literature references a.) Water [9], and b.) Ethanol [10].

azimuthal positions of the analyzer rather than continuously during rotation.

The resulting complex refractive indices (Figure 3.) are in good accordance with the literature values [9, 10], considering that the former attempts to determine the refractive index from the extinction coefficient ($k$) by the means of the Kramers–Kroenig relations [11], where the extinction coefficients were calculated from the measured absorbance in transmission. While several newer datasets for water exist [12, 13], they show non-negligible discrepancies with one another across portions of the mid-IR. Consequently, selecting a single dataset as a definitive benchmark for comparison with spectroscopic ellipsometry (SE) results is not straightforward. Data from Segelstein et al. [9] remains a widely used baseline.

In Figure 3, the refractive index and extinction coefficient of the water and ethanol are presented respectively. For the ethanol in the C–H stretching region (around 3000 $cm^{-1}$), we observe small deviations relative to the reference dataset. This region is sensitive to sample condition (ethanol is hygroscopic; minor water uptake or trace impurities can influence the band shape) and to temperature. In addition, finite opening-angle averaging and the use of a compact effective dispersion parametrization can lead to small differences compared to literature optical constants obtained under different experimental conditions.

The refractive indices of the mixtures are coming from fits on the concentration series elements by the Lorentz-Lorenz type effective medium (LL) [11], combining the water and ethanol dispersions Figure 4. The LL relation is used here as a compact, effective parameterization to describe the concentration series.

The formula for the LL-EMA type mixing for effective dielectric function:

$$\frac{\varepsilon_{eff}-1}{\varepsilon_{eff}+2}=f\frac{\varepsilon_e-1}{\varepsilon_e+2}+(1-f)\frac{\varepsilon_w-1}{\varepsilon_w+2},$$

where $\varepsilon_{eff}$ is the effective dielectric function of the mixture, $\varepsilon_e$ and $\varepsilon_w$ are the dielectric functions of the ethanol and water, respectively, while $f$ is the ethanol volume fraction.

For water–ethanol mixtures in the mid-IR, molecular interactions (e.g., hydrogen bonding) can modify the spectral response, therefore LL should not be interpreted as a molecular-level non-interacting “dry-component” mixing model. In this work, LL is applied to obtain an effective concentration parameter from the ellipsometric response, suitable for tracking controlled composition changes. Both the water and the ethanol ellipsometry measurement results were fitted by a combination of a Sellmeier dispersion law

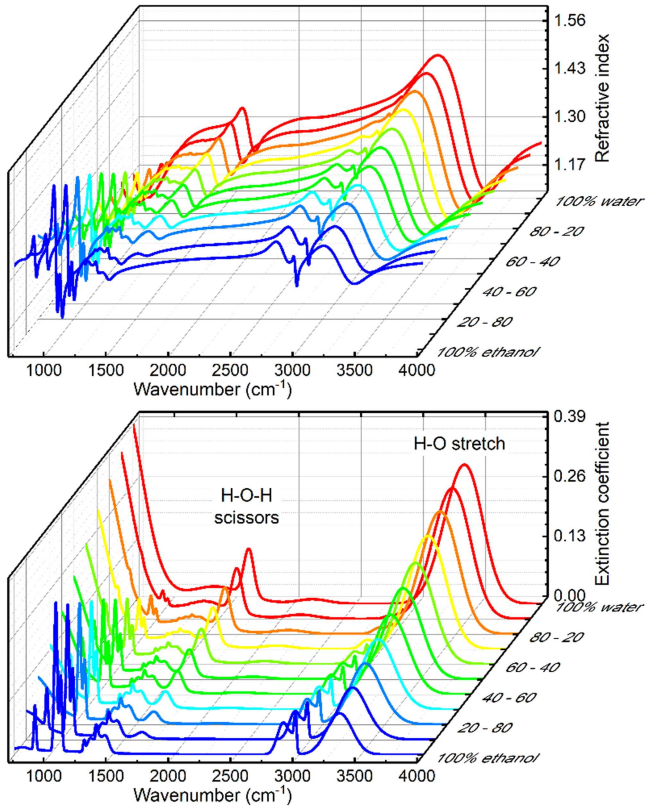


**FIGURE 4** | Refractive index and extinction coefficients of the Water–Ethanol mixture components (by measured volumes of the components).

component and a series of Gauss oscillators [11]. Specifically, we used 5 Gaussian oscillators plus one Sellmeier component for water and 18 Gaussian oscillators plus one Sellmeier component for ethanol. Remaining discrepancies may be caused by contamination during sample handling/exposure to ambient conditions and by temperature differences. In addition, the finite opening angle leads to angular averaging, which can introduce small deviations from idealized single-angle modeling. We therefore report goodness-of-fit metrics and focus on robust relative changes in n and k under controlled composition variation. Narrow features due to residual atmospheric $CO_2$ absorption are present in the mid-IR data. During the dispersion fitting, the affected spectral intervals were excluded from the optimization to avoid biasing the extracted optical constants. The stability of the results was confirmed by varying the exclusion windows and monitoring goodness-of-fit and the resulting n and k. The parametric models yielded the $R^2 = 0.9547$ for the ethanol and $R^2 = 0.9919$ for water. An additional surface layer was included in the optical model to obtain slightly better fits. This surface layer was a Bruggeman-type effective medium composed of the underlying solution (~2%) and air.

In Figure 5. the Lorentz–Lorenz EMA concentration parameter is plotted versus the w% of the water–ethanol mixtures, which indicates a monotone growing curve, providing the possibility to apply the method for w% concentration determination for water–ethanol-based solutions such as chemical products or alcoholic beverages.

In Figure 5, the x-axis shows the measured/prepared mass fraction (w%), while the y-axis shows the LL-derived volume fraction (v%) obtained from the fitted parameter *f*. Since mass fraction and volume fraction are not linearly related (due to different densities), a non-linear relationship is expected. Non-ideal mixing (e.g., volume contraction) may further contribute to deviations from linearity.

The second investigated system is the solution of NaCl in water. The expectation is that the dissolved ions of the NaCl locally distort the random orientation of water molecules and arrange them around the $Na^+$ and $Cl^-$ ions, also introducing a change in the complex refractive index of the solution Figure 6. At 25°C, there is a saturation concentration for this system at 26.47 w% [8].

By following the refractive index values at an arbitrary wavelength, which was selected as 1000 $cm^{-1}$ (10 μm), the sensitivity of the method can be observed Figure 7. The low concentration behavior of the refractive index is related to the hydrogen-bound network topology in water [14].

For the NaCl(aq) series, the dispersion of saline water was modeled using five Gaussian oscillators and one Sellmeier term. To ensure fit stability and limit parameter correlations, only a subset of parameters was fitted. For the two strongest and the fourth-strongest Gaussian oscillators, amplitude, center position, and broadening were fitted. For the third-strongest oscillator, only amplitude and broadening were fitted, while the center position was fixed. The weakest Gaussian oscillator was kept fixed. For the Sellmeier contribution, only the B parameter was fitted.

To ensure numerical stability and limit parameter correlations, the dispersion fitting was performed using a constrained strategy in which only a subset of physically relevant parameters was allowed to vary. Initial oscillator positions and widths were estimated from the measured spectra and established infrared spectroscopy literature, and were refined iteratively. Increasing model complexity beyond the final

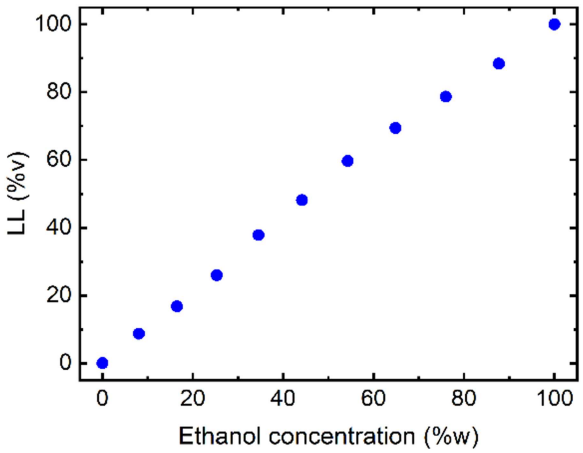


**FIGURE 5** | Correlation between ethanol mass fraction (w%, x-axis) and the Lorentz–Lorenz (LL)–derived effective ethanol volume fraction (v%, y-axis) obtained as the single LL-EMA composition parameter from spectral fitting.

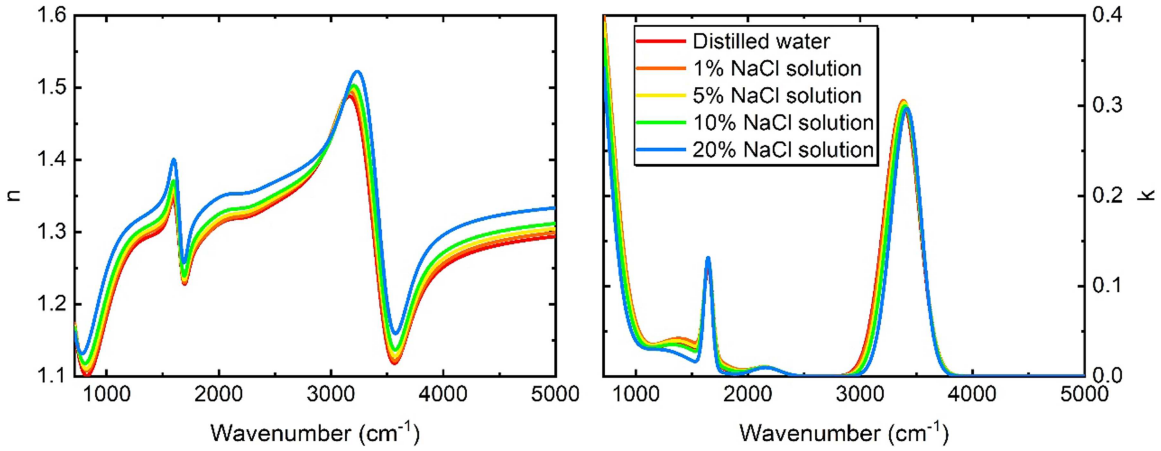


**FIGURE 6** | Derived refractive index values obtained from fitted optical models. Refractive index ($n$) and extinction coefficients (k) of the various concentrations of NaCl solutions in water.

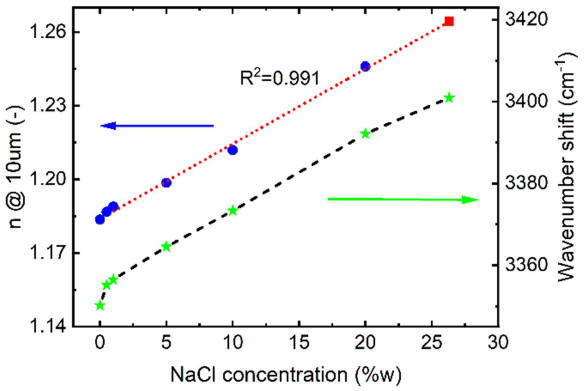


**FIGURE 7** | Blue dots show the NaCl-water solution refractive indices obtained from fitted optical models at 10 μm wavelength (2000 $cm^{-1}$ wavenumber). The red square shows the refractive index of the solution at saturation concentration.

configuration did not alter the observed concentration-dependent trends, but led to increased parameter correlation and reduced fit robustness. Therefore, a compact parameterization was deliberately preferred.

By fitting a linear curve to the linear range of the 1–20% concentrations, the saturation values of the concentration could be predicted. The fit provides the following equation for the concentration:

$$C = 327.87n - 388.17$$

Substituting the measured refractive index of the saturated NaCl solution (1.2645) into the above equation provides $C_{saturation} = 26.45$ w%, which is in good match with the saturation concentration of NaCl in water [8].

As the fitting result provides numerical data for the signature water peaks, we can investigate quantitatively the effect of the salt concentration on the possible shifts of these peaks. The maximum of the scissors and stretching mode peaks are at 1642.6 $cm^{-1}$ (6.087 μm) and 3350.2 $cm^{-1}$ (2.985 μm), respectively. Comparing the peaks maxima of the saturated solution and the water, the stretching mode peak shows 50.7 $cm^{-1}$ (0.0445 μm) maximal shift while the scissors mode shows a negligible shift compared to the former.

Salt–water interactions are well known to perturb the hydrogen-bond network and thus modify the stretching-region vibrational response of water, as reported in FTIR and Raman studies of aqueous alkali halide solutions [15, 16]. Our finding of a pronounced concentration-dependent shift in the stretching region, accompanied by only negligible shifts in the bending region, is consistent with these literature observations.

The approximately linear relationship between refractive index and NaCl concentration is valid within the investigated 1–20 wt % range and forms the basis of the proposed sensing approach. Near the saturation limit, deviations from linearity are expected due to increased ion–water interactions and non-ideal solution behavior. Therefore, the method is most reliable within the sub-saturation regime, while measurements close to saturation should be interpreted with caution.

## 4 | Summary

The above study showed that the method developed for visible ellipsometry to perform measurements on liquid surfaces is also appropriate for FTIR-type mid-IR range ellipsometry, for which the measurement time is longer due to its different data collection principle. The measurement results of the two investigated systems of water alcohol mixtures and saline water solutions showed sensitivity for the concentration ladders applied in the experiments, providing a label-free, contactless optical method for investigating organic and inorganic liquids and liquid solutions.

**Acknowledgements**

This research was funded by the National Research, Development and Innovation Office (NKFIH) in Hungary through the Grants Nr. K-146181. Project no. TKP2021-EGA04 has been implemented with support from the Ministry of Innovation and Technology of Hungary, from the National Research, Development and Innovation Fund, financed under the TKP2021 funding scheme. On behalf of the

'MFA-Fotonika-1' project, we are grateful for the possibility of using the HUN-REN Cloud.

## Data Availability Statement

The data that support the findings of this study are available from the corresponding author upon reasonable request.

## Conflicts of Interest

The authors declare no conflicts of interest.

## References

1. L. Makai, B. Kalas, and G. Tiborcz, "Spectroscopic Ellipsometry Investigation of Free Liquid-Liquid and Liquid-Air Interfaces," *Thin Solid Films* 764 (2023): 139634, https://doi.org/10.1016/j.tsf.2022.139634.

2. K. Hinrichs and K.-J. Eichhorn, *Ellipsometry of Functional Organic Surfaces and Films* (Springer Nature, 2018). 2nd edn.

3. C. Kratz, A. Furchner, G. Sun, J. Rappich, and K. Hinrichs, "Sensing and Structure Analysis by in Situ IR Spectroscopy: From mL Flow Cells to Microfluidic Applications," *Journal of Physics: Condensed Matter* 32 (2020): 393002, https://doi.org/10.1088/1361-648X/ab8523.

4. A. Röseler, "11 - Spectroscopic Infrared Ellipsometry." in *Handbook of Ellipsometry*, eds. Harland G. Tompkins and Eugene A. Irene. (William Andrew Publishing, 2005), 763–798.

5. L. Makai, T. Lehto, B. Fodor, and P. King, "Breakthrough Instruments and Products: Investigation of Atomic Layer Deposited Al:ZnO Layer by Spectroscopic Ellipsometry From the Deep-UV to the Mid-IR in One Instrument," *Review of Scientific Instruments* 92, no. 11 (2021): 119501.

6. M. R. Querry, W. E. Holland, R. C. Waring, L. M. Earls, and M. D. Querry, "Relative Reflectance and Complex Refractive Index in the Infrared for Saline Environmental Waters," *Journal of Geophysical Research* 82, no. 9 (1977): 1425–1433, https://doi.org/10.1029/JC082i009p01425.

7. J. Burgess, *Metal Ions in Solution*. (Ellis Horwood, 1978).

8. W. M. Haynesed, *CRC Handbook of Chemistry and Physics*. (CRC Press LLC, 2014), 4–89.

9. D. J. Segelstein. The Complex Refractive Index of Water, Master Thesis (1981).

10. E. Sani and A. Dell'Oro, "Spectral Optical Constants of Ethanol and Isopropanol From Ultraviolet to Far Infrared," *Optical Materials* 60 (2016): 137–141.

11. H. Fujiwara, *Spectroscopic Ellipsometry: Principles and Applications* (John Wiley & Sons, 2007).

12. J.-J. Max and C. Chapados, "Isotope Effects in Liquid Water by Infrared Spectroscopy. III. $H_2O$ and $D_2O$ Spectra From 6000 to 0 $cm^{-1}$," *Journal of Chemical Physics* 131 (2009): 184505.

13. J. Fiedler, M. Boström, C. Persson, et al., "Full-Spectrum High-Resolution Modeling of the Dielectric Function of Water," *Journal of Physical Chemistry. B* 124, no. 15 (2020): 3103–3113.

14. I. Bakó, Á. Bencsura, K. Hermannson, et al., "Hydrogen Bond Network Topology in Liquid Water and Methanol: A Graph Theory Approach," *Physical Chemistry Chemical Physics* 15 (2013): 15163–15171.

15. Z. S. Nickolov and J. D. Miller, "Water Structure in Aqueous Solutions of Alkali Halide Salts: FTIR Spectroscopy of the OD Stretching Band," *Journal of Colloid and Interface Science* 287, no. 2 (2005): 572–580, https://doi.org/10.1016/j.jcis.2005.02.001.

16. C. C. Holzammer and A. S. Braeuer, "Raman Spectroscopic Study of the Effect of Aqueous Salt Solutions on the Inhibition of Carbon Dioxide Gas Hydrates," *Journal of Physical Chemistry B* 123, no. 10 (2019): 2354–2361.